

## Spatial and temporal variability of satellite-derived sea surface temperature in the Barents Sea

Mateusz Jakowczyk<sup>a</sup> and Malgorzata Stramska<sup>a,b,\*</sup>

<sup>a</sup>Department of Earth Sciences, Szczecin University, Szczecin 70-383, Poland; <sup>b</sup>Institute of Oceanology, Polish Academy of Sciences, Sopot 81-712, Poland

(Received 6 April 2014; accepted 4 June 2014)

The Barents Sea (BS) is an important region for studying climate change. This sea is located on the main pathway of the heat transported from low to high latitudes. Since oceanic conditions in the BS may influence vast areas of the Arctic Ocean, it is important to continue to monitor this region and analyse the available oceanographic data sets. One of the important quantities that can be used to track climate change is the sea surface temperature (SST). In this study, we have analysed the 32 years, (1982–2013) National Oceanic and Atmospheric Administration (NOAA) Optimum Interpolation SST Version 2 data for the BS. Our results indicate that the regionally averaged SST trend in the BS (about  $0.03^{\circ}\text{C year}^{-1}$ ) is greater than the global trend. This trend varies spatially with the lowest values north from  $76^{\circ}\text{N}$  and the highest values (about  $0.06^{\circ}\text{C year}^{-1}$ ) in proximity of Svalbard and in coastal regions near the White Sea. The SST and 2 m air temperature (AT) trends are high in winter months in the open BS region located west from Novaya Zemlya. Such trends can be linked to a significant retreat of sea ice in this area in recent years. In this article, we also documented spatial patterns in the annual cycle of SST in the BS. We have shown that the interannual variability of SST is similar in different regions of the BS and well correlated with the interannual patterns in AT variability.

### 1. Introduction

The Barents Sea (BS) is the northernmost Arctic shelf sea with surface partly free of sea ice even during the winter season. The BS is an important region for studying climate change and interactions between the atmosphere, the sea ice, and the ocean. This rather small and shallow sea (an area about 10% of the Arctic Ocean and an average depth about 230 m) has a great influence on the entire Arctic, as this region is located on the main pathway of the heat transported by the ocean from low to high latitudes. The relatively warm Atlantic water (AW) in the Norwegian Atlantic Current (NAC) is exposed in the BS to the cold air, efficiently cooled, and vertically mixed (Maslowski et al. 2004; Rudels et al. 2004; Schauer et al. 2002, 2008). The loss of heat from the ocean creates cool and dense water that sinks, transporting  $\text{CO}_2$  sequestered from the atmosphere. Water mass transformations in the BS are reinforced by the brine rejection processes that occur during sea-ice formation, and as a result, the deep waters are ventilated more effectively than in any other Arctic shelf sea (Schauer et al. 2002). The oceanographic processes within the BS have a documented influence on the entire Arctic region and contribute significantly to the overall overturning in the Atlantic Ocean. It has been estimated that more than 50% of the Arctic Ocean winter heat loss occurs in the BS (Serreze et al. 2007).

---

\*Corresponding author. Email: [mstramska@wp.pl](mailto:mstramska@wp.pl)

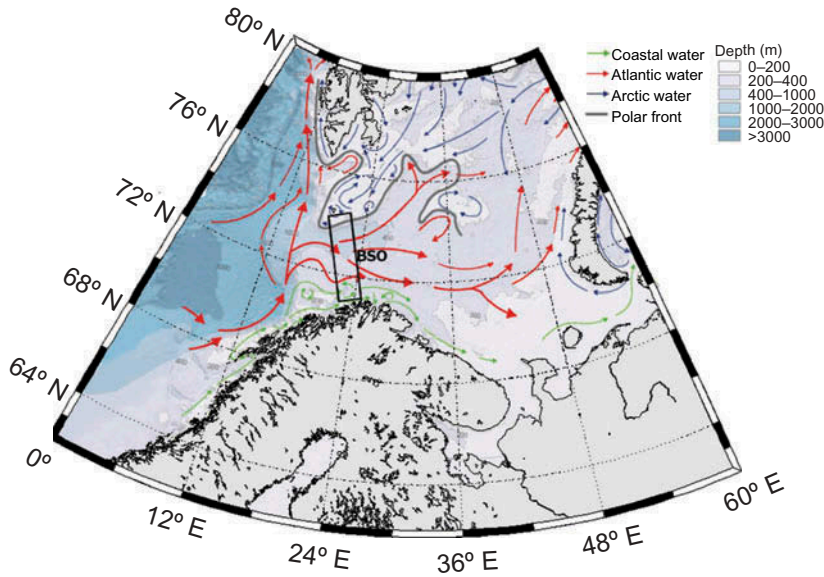


Figure 1. Map showing the main features of the bathymetry and surface currents in the Barents Sea. Approximate position of the Barents Sea Opening (BSO) is indicated by a box.

Physical oceanographic conditions in the BS depend significantly on the inflow of AW, which takes place through the southwestern BS boundary between Bjørnøya (Bear Island) and Fugløy, often called the Barents Sea Opening (BSO, Figure 1). Some of the inflowing AW recirculates within the Bear Island Trough, but most of it passes through the BS and exits through the strait between Novaya Zemlya and Franz Josef Land (Loeng 1991). A series of causes and effects involved in the air–sea interactions have been described in the published literature. In particular, the positive feedback loops operating in the Barents system have been suggested. One of the feedback loops has been associated with an anomalously high transport of heat in the BS due to the increased volume transport and/or temperature of the AW. This leads to a warmer BS and requires more cooling for freezing; therefore, in years when this happens, less winter sea ice is usually formed (Sandø et al. 2010; Schlichtholz 2011). Larger temperature difference between the cold air and the warm ocean during this scenario leads to an increased net surface heat loss from the ocean to the atmosphere (Ikeda 1990; Ådlandsvik and Loeng 1991). The increased heat flux from the ocean warms the lower atmosphere, which can result in the cyclonic circulation anomaly with strong westerly winds over the BS. This in turn can increase even more the inflow of the warm AW to the BS. This feedback loop is considered to be stable and self-maintaining (Ådlandsvik and Loeng 1991; Schlichtholz and Houssais 2011). Another positive feedback loop has been attributed to a large portion (>60%) of the BS inflow being transformed into the cold deep water (CDW) with temperatures below 0°C (Midttun 1985; Schauer et al. 2002). These waters sink and leave the BS region between the Franz Josef Land and Novaya Zemlya. This feedback loop operates in such a way that in years with greater heat loss to the atmosphere, a larger amount of denser CDW is created, which results in an increased deep water outflow. This in turn favours a larger inflow of AW to the BS, through the barotropic forcing. Thus, the increased AW inflow is part of the ‘common axis’ of both feedback loops, stimulating less sea ice and more heat loss to the atmosphere. Atmospheric responses to the large surface heat loss in the BS have been proposed as one way

to maintain the decadal oscillations in the Arctic system (Ikeda 1990; Ikeda, Wang, and Zhao 2001; Bengtsson, Semenov, and Johannessen 2004).

Since oceanic conditions and long-term climatic trends in the BS may be indicative of the overall climate change in the Arctic Ocean and the exact mechanisms behind these changes are still being debated, it is important to continue to monitor this region and analyse the available oceanographic data sets. In this article, we focus on the sea surface temperature (SST) data records covering 32 years (1982–2013). We document long-term SST trends and their regional variability. We also discuss characteristic features of the annual SST cycle, interannual, and short-term variability. The information about SST is important for improved understanding of the BS. The SST has been classified as one of the Essential Climate Variables that support the work of the Intergovernmental Panel on Climate Change and the UN Framework Convention on Climate Change. In particular, the exchange of heat between the atmosphere and the ocean depends strongly on this single oceanic quantity (as well as on atmospheric parameters such as wind speed, air temperature (AT), humidity, and cloudiness). Patterns of SST variability on interannual and longer timescales have been associated with important modes of climate variability in various geographical regions such as the North Atlantic Oscillation, the Arctic Oscillation, the El Niño–Southern Oscillation, the Pacific Decadal Oscillation, and the Atlantic Multidecadal Oscillation (Deser et al. 2010). Better understanding of SST patterns and variability in the BS can significantly improve our understanding of the climate changes happening currently in this region.

## 2. Data sources and methods

This study is based on satellite-derived SST data. Satellite remote sensing has established itself as an indispensable technique of acquiring global information about oceans. Difficulties due to the rough weather and harsh conditions yield a general lack of systematic long-term *in situ* measurements in the Arctic. The spatial distribution of the *in situ* monitoring network in the Arctic is uneven, and large areas of the Arctic remain essentially unmonitored. Limited availability of *in situ* data is a serious impediment to the development of in-depth understanding of variability and long-term trends in this region. Therefore, satellite remote sensing is a method of particular importance in Arctic research.

For our study, we have selected the 32 year long data series (years 1982–2013) known as the National Oceanic and Atmospheric Administration (NOAA) Optimum Interpolation SST Version 2 data set (Reynolds et al. 2007). These SST data were provided by the NOAA/OAR/ESRL PSD, Boulder, Colorado, through their website at <http://www.esrl.noaa.gov/psd/>. These are daily records, with spatial resolution of approximately  $0.25^\circ \times 0.25^\circ$ . Advanced Very High Resolution Radiometer (AVHRR) infrared satellite measurements were used to derive these SST estimates (Pathfinder data: from September 1981 to December 2005; operational AVHRR: January 2006 onwards). In addition, *in situ* data from ships and buoys were used for a large-scale adjustment of satellite biases with respect to the *in situ* data. Full details of the data processing and day-to-day analyses of the differences between the derived data set and the *in situ* measurements from ships and moorings are provided in the study by Reynolds et al. (2007). Although the Reynolds data have been verified slightly unstable in time (Liang and Ignatov 2011), this is currently the longest satellite data record that can be used to study the long-term SST trends and variability.

Our main interest in this article is in the BS, but maps presented in Section 3 cover also the vicinity of the BS to show a better perspective for the analysed SST variability. In some cases, we refer to ‘BS averaged’ quantities, for example SSTs. In this case, we mean that the data have been averaged over the region between  $0^\circ$  E  $62.875^\circ$  N and  $59.875^\circ$  E

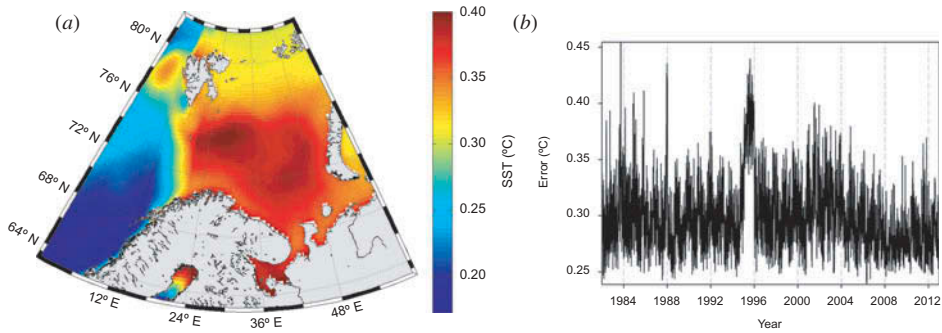


Figure 2. (a) Regional distribution of the total SST error averaged in 32 years (1982–2013). (b) Time series of the total SST error averaged over the BS region ( $0^{\circ}$  E  $62.875^{\circ}$  N;  $59.875^{\circ}$  E  $82.375^{\circ}$  N).

$82.375^{\circ}$  N. For discussion of the geographical variability, we also use averages representing smaller geographical regions. For this purpose, we have defined four regions (Figure 3): region 1 (SW) located between  $0.625^{\circ}$  E,  $63.125^{\circ}$  N,  $19.125^{\circ}$  E,  $73.125^{\circ}$  N, region 2 (SE) located between  $21.125^{\circ}$  E,  $69.125^{\circ}$  N,  $42.125^{\circ}$  E  $74.125^{\circ}$  N, region 3 (NW) located between  $3.125^{\circ}$  E,  $74.125^{\circ}$  N,  $17.125^{\circ}$  E  $79.625^{\circ}$  N, and region 4 (NE) located between  $24.125^{\circ}$  E,  $76.125^{\circ}$  N,  $47.625^{\circ}$  E  $78.125^{\circ}$  N. For brevity, we use terms such as ‘region SW averages’ in this article. In all cases, the regional averages were calculated only from pixels representing ocean surface.

The SST data set includes complementary information about the total SST error and the sea-ice fraction for each pixel. The total error is derived from random sampling and bias error (Reynolds et al. 2007). We have plotted the average error (in years 1982–2013) in Figures 2(a) and (b). As can be seen in Figure 2(a), the average error is relatively small in the region of the NAC (about  $0.25^{\circ}\text{C}$ ) and it increases in the central area of the BS to about  $0.4^{\circ}\text{C}$ . Time series of the total SST error averaged over the BS presented in Figure 2(b) indicate that the error was highest in 1998.

In addition to the SST data, we have also examined meteorological data from the NOAA-CIRES Climate Diagnostic Center NCEP/NCAR (National Centers for Environmental Prediction and National Center for Atmospheric Research) Reanalysis 1. The Reanalysis Project employs a state-of-the-art analysis/forecast system to assimilate global meteorological data from various available sources from 1948 to the present. In this article, we have included comparisons of the SST data with the daily data of 2 m AT. These data have coarser spatial resolution than the SST data and are provided on the  $2.5^{\circ} \times 2.5^{\circ}$  spatial grid.

Standard statistical methods were used to derive trends and to test for statistical significance (Ostasiewicz, Rusnak, and Siedlecka 2006).

### 3. Results and discussion

#### 3.1. Average and extreme SST

In Figure 3, we have plotted the 32 year-averaged SST for the region of the BS. Visual comparison of Figure 3 with Figure 1 leads to the conclusion that there is a lot of similarity between the spatial SST distribution and spatial patterns of surface currents shown in Figure 1, as expected. The highest 32 year average SST value ( $>8^{\circ}\text{C}$ ) is observed in the NAC, while the lowest average SST values (below  $0^{\circ}\text{C}$ ) are present in the northeastern parts of the BS, a region that is covered by sea ice in winter.

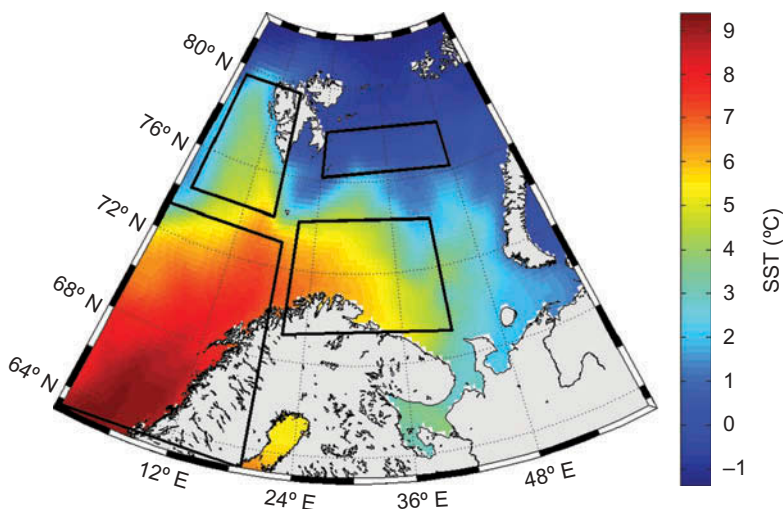


Figure 3. Map of the 32 year (1982–2013) averaged SST in the study region. Black boxes indicate the four study regions discussed in the text.

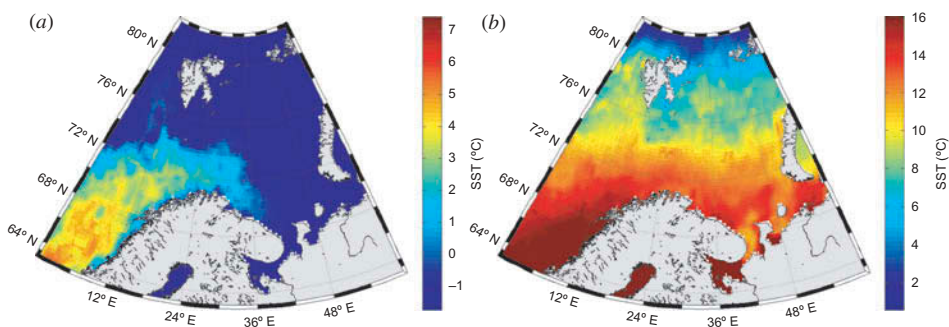


Figure 4. Extreme SST values: (a) map of the minimum SST, (b) map of the maximum SST, observed at each pixel in the time period between 1 January 1982 and 31 December 2013. Note that the colour scale is different at each plot.

Figure 4 shows maps of the extreme temperatures (minimum and maximum) observed in the entire 32 year long SST data record. As anticipated, the highest minimum and maximum temperatures are associated with the NAC, with the maximum temperatures exceeding 20°C. The lowest SST values occur in the northeastern part of the region, where sea ice is present during winter months. Generally, the temperatures decrease with the distance from the NAC. Spatial patterns of SST displayed in Figures 3 and 4 served as a basis for defining the four subregions indicated in Figure 3 by boxes. We compare some of the characteristic features of the SST variability in these four regions later.

### 3.2. Seasonal cycle

The most prominent characteristic feature of the SST variability in our study region is the seasonal cycle. This is summarized in Figures 5 and 6. In Figure 5(a), we display a spatial

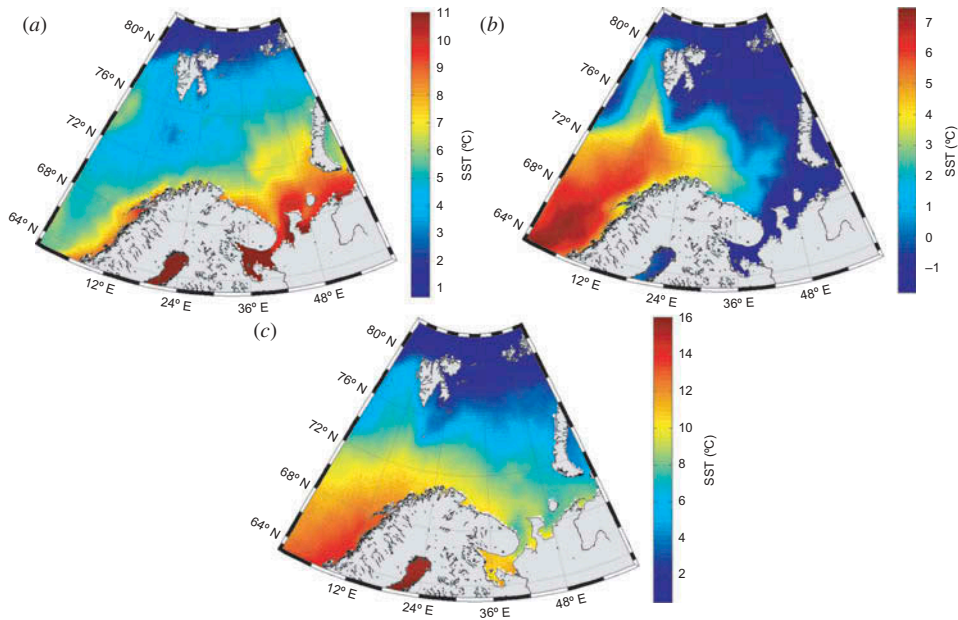


Figure 5. Summary of the 32 year averaged annual cycle of SST: (a) amplitude, (b) minimum, and (c) maximum SST estimated for the 32 year averaged annual cycle. Note that the colour scale is different at each plot.

distribution of the 32 year averaged amplitude of the annual cycle. The minimum and maximum SST values of the 32 year averaged annual cycle are plotted in Figures 5(b) and (c). Note that the colour scale is different for every figure, to show the range of SST values better. As can be seen in Figure 5(a), the greatest amplitude of the seasonal SST cycle (more than 8°C) is associated with the coastal regions (Norway, Kola peninsula, northern part of Russia) and with the shallow section of the BS where the water depth is below 200 m. The smallest amplitude of the 32 year averaged annual SST cycle (about 3°C) is observed in the northern regions and in the West Spitsbergen current. The highest minimum and maximum SST values of the 32 year averaged annual cycle (7°C and 13°C, respectively) are noted in the region of the NAC. The dates when the minimum and maximum SST values of the 32 year averaged annual cycle are observed are shown in Figures 6(a) and (b), respectively. In large areas of the BS, the minimum SST values of the 32 year averaged annual cycle occur as late as in March and April, while the maximum SST values are observed most often in August.

The seasonal cycle is also summarized in Figure 7 as the time series of the 32 year mean SST averaged in our four study regions. For comparison, we have plotted in Figure 7 time series of the 32 year averaged 2 m ATs. If we define the ‘warm season’ as the time of the year when SST is greater than the annually averaged SST, we can say that the 32 year mean annual SST cycle is asymmetric, with the ‘cold season’ lasting about 7 months from November till mid-June and the ‘warm season’ lasting for 5 months from June to the end of October. The longest ‘warm season’ is observed in the SW region. The standard deviations (SDs) (not shown in Figure 7) of the daily SST values in the 32 year series assume higher values (about 1°C) for the NE region in the warmest months of the year and lower values (about 0.5°C and less) in the SW region in April. The range

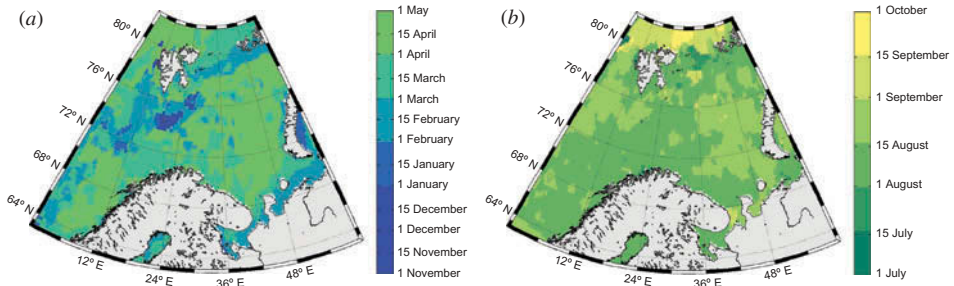


Figure 6. Summary of the 32 year averaged annual cycle of SST: (a) day of the year when the minimum SST is observed and (b) day of the year when the maximum SST is observed.

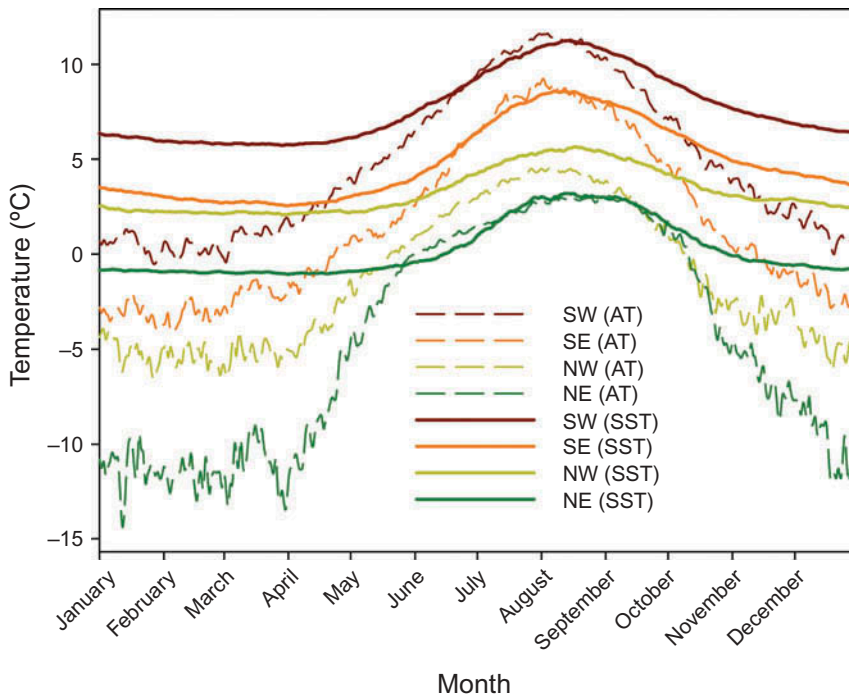


Figure 7. The 32 year averaged annual cycle of SST (solid line) and AT (dashed line) in the four study regions. The geographical positions of each of the regions are shown in Figure 3.

of the AT values is greatest in the NE region and smallest in the NW region. The time period when the 32 year average AT is above 0°C is the longest in the SW region (March–January) and the shortest in the NE region (June–October). Comparison of SST and AT data displayed in Figure 7 leads to the conclusion that the seasonal increase in the AT leads to the seasonal increase in the SST in all regions (by about 30 days). The 32 year averaged ATs in each region appear to be lower than the corresponding SST temperatures most of the time. This observation underlines the fact that the BS is a region of significant heat loss from the ocean to the atmosphere.

### 3.3. Longer-term changes

Time series of annually averaged SST data have been used to estimate the 32 year SST trends in the region of the BS, presented in Figure 8(a). From the results shown in Figure 8, we conclude that the trends of increasing annual mean SST (statistically significant at 95% confidence level,  $p < 0.05$ ) are high in the regions adjacent to the western part of the Hopen Island, where they assume values of about  $0.06^{\circ}\text{C year}^{-1}$  (or  $0.6^{\circ}\text{C per decade}$ ) and in the coastal regions of the White Sea (about  $0.08^{\circ}\text{C year}^{-1}$ ). The trends in annually averaged SST are low or insignificant in the northern region of the BS. For comparison, according to Good et al. (2007), the rate of globally averaged SST (calculated for 20 years of AVHRR Pathfinder data from January 1985 to December 2004) has been estimated to be  $0.18^{\circ}\text{C}$  and  $0.17^{\circ}\text{C}$  per decade from daytime and night-time data, respectively. The warming trends estimated by us in the BS are greater than these global trends in most of the regions located south from  $76^{\circ}\text{N}$ . Large SST trends observed in the coastal regions can be associated with increasing water run-off from land in the Arctic (e.g. Peterson et al. 2002), which can provide the source of water warmer than the ocean coastal waters (Nghiem et al. 2014). In addition, increased input of freshwater increases water column stratification in the ocean (e.g. Morison et al. 2012; Lesack et al. 2014) and supplies more terrigenous material, which decreases water transparency and increases surface water heating (Fichot et al. 2013).

In order to investigate the seasonal dependence of the SST trends, we have also calculated the 32 year trend for the SST data averaged for January–February (winter months) and July–August (summer months). These trends are shown in Figures 8(b) and (c), respectively. The comparison of these two figures leads to the conclusion that there is

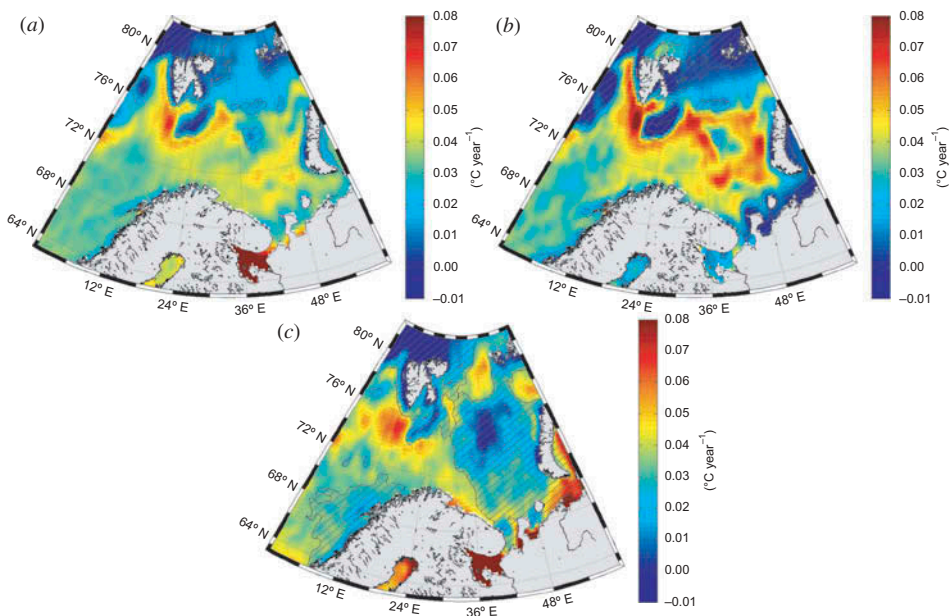


Figure 8. Trends in the SST records based on the time series from 1982 to 2013: (a) trends for the annual mean SST, (b) trends for the SST averaged in the months of January and February, and (c) trends for the SST averaged in the months of July and August. Only in the area that is not hatched the trends are statistically significant ( $p < 0.05$ , 95% confidence level).

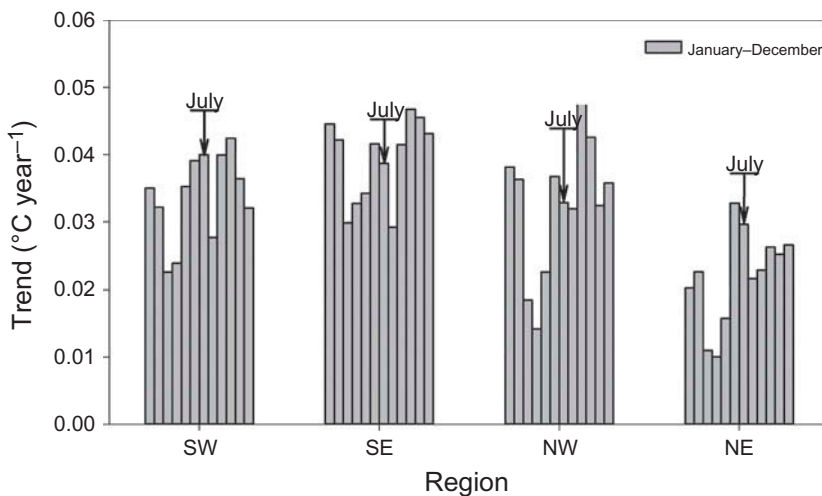


Figure 9. Trends in the monthly SST data averaged in the four study regions.

a significant seasonal variability of the long-term trends. In the open waters, the trends are the greatest in the winter months. The SST trends have been also estimated for every month of the year in each of the study regions, and the results are shown in Figure 9. As can be seen, on average, the trends in all regions have generally low values in March and April, and the trends in the NE region are lower than the trends in the other regions.

The trends estimated from SST data can be compared with similar regional trends of marine AT at 2 m presented in Figure 10. Note that since the 2 m daily AT NCEP data are provided on the grid of  $2.5^{\circ} \times 2.5^{\circ}$ , the pixels shown in Figure 10 are significantly larger than the pixels in our SST maps. The comparison of the SST and AT trends reveals that the spatial patterns of these trends are rather different. However, the AT trends reach the highest values of about  $0.2^{\circ}\text{C year}^{-1}$  in the winter months in the region located east from Svalbard Archipelago (between the Franz Josef Land and Novaya Zemlya). This is approximately the same region where we observed the highest values of the SST trends (Figure 8), although the SST trends have lower values than the AT trends. This open BS region is associated with a significant retreat of the sea ice in recent years. This is illustrated in Figure 11, which compares the spatial distribution of the sea-ice concentration observed in the winter months (January–April) of 1982 and 2013. One can clearly see that the area of the open BS where the sea ice has not been observed in the winter of 2013 is significantly larger in comparison to the area not covered by the sea ice in the winter of 1982. Thus, the increased trends in the SST and AT can be linked to the decrease in the sea surface albedo when the sea ice is vanishing. This explanation is in line with the similar observation made recently by Comiso and Hall (2014) and based on data sets for the entire Arctic.

Interannual patterns of SST and AT variability are summarized in Figures 12 and 13, which show the temperature anomalies calculated by subtracting the seasonal cycle component from the daily data and by averaging the daily anomalies into the annually averaged anomalies. Next, these anomalies were also averaged spatially in the four regions. Multi-year trends were not subtracted. In Figures 12(a) and (b), we compare the time series of the annual SST and AT anomalies in the four regions, respectively. The temporal variations of the SST anomalies (Figure 12(a)) are similar in all regions. The

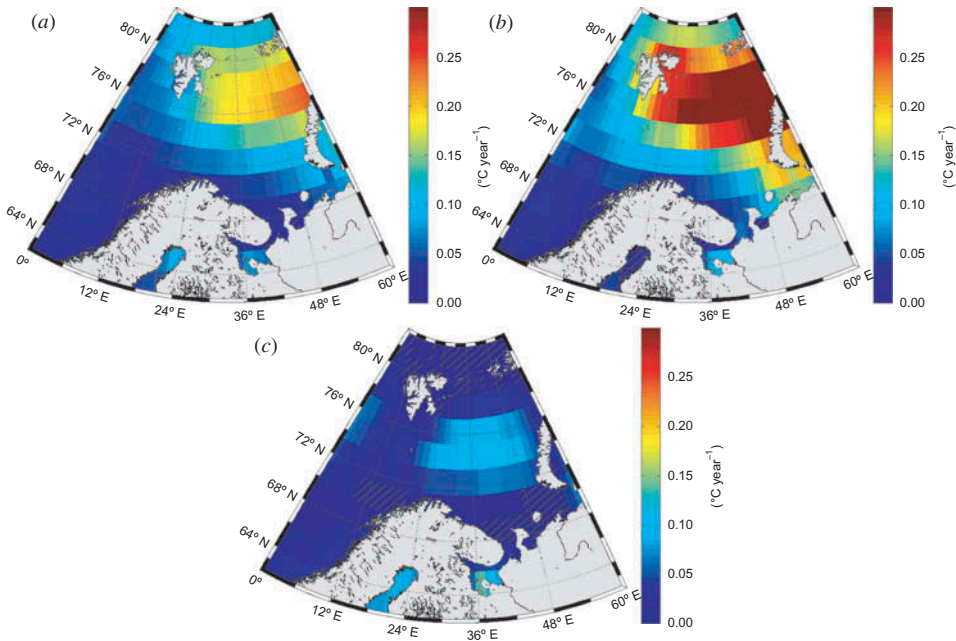


Figure 10. Trends in the time series of the air temperature (AT) based on data from 1982 to 2013: (a) trends for the annual mean AT, (b) trends for the AT averaged in the months of January and February, and (c) trends for the AT averaged in the months of July and August. Trends are not statistically significant ( $p < 0.05$ , 95% confidence level) only in the small hatched regions to the north and south.

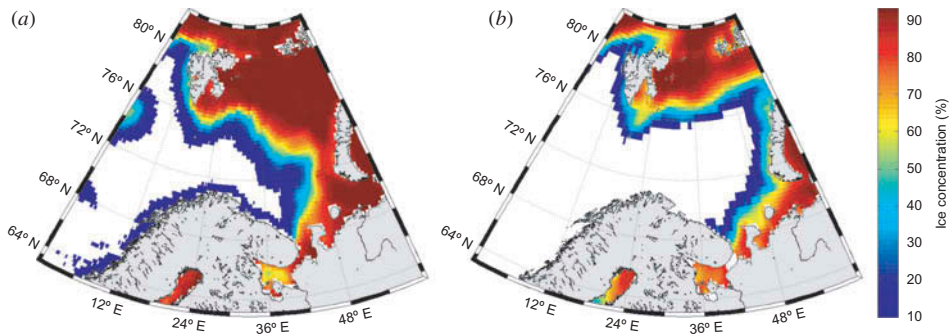


Figure 11. The concentration of the sea ice (%) averaged in (a) January–April 1982 and (b) January–April 2013.

variations of the AT anomalies (Figure 12(b)) seem to be generally larger than the variations of the SST anomalies, and in particular in the NE region, they assume notably larger values than in all other regions. The annual SST and AT anomalies intercompared at each region separately show similarities in their temporal patterns (Figure 13). This is also supported by the results shown in Figures 14 and 15. In Figures 14(a)–(c), the correlations between SST anomalies in the SW region and the other three regions are summarized. The best correlation has been found between SW and SE regions ( $r = 0.75$ ), whereas the

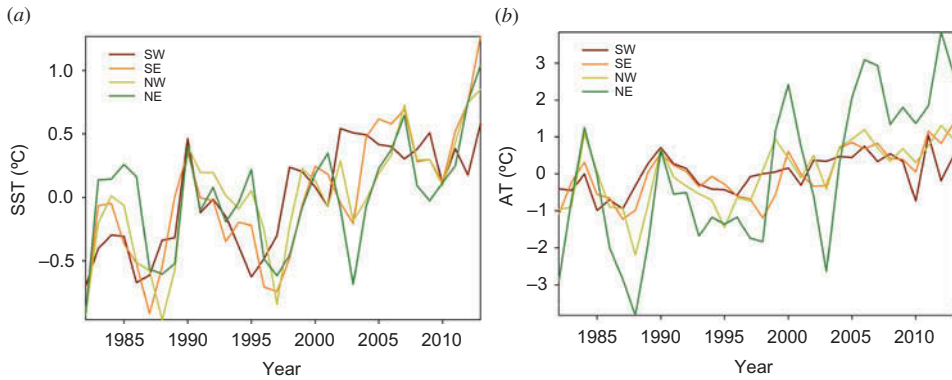


Figure 12. Time series of the annual (a) SST anomalies and (b) AT anomalies, averaged in the four study regions. Geographical positions of each of the regions are shown in Figure 2.

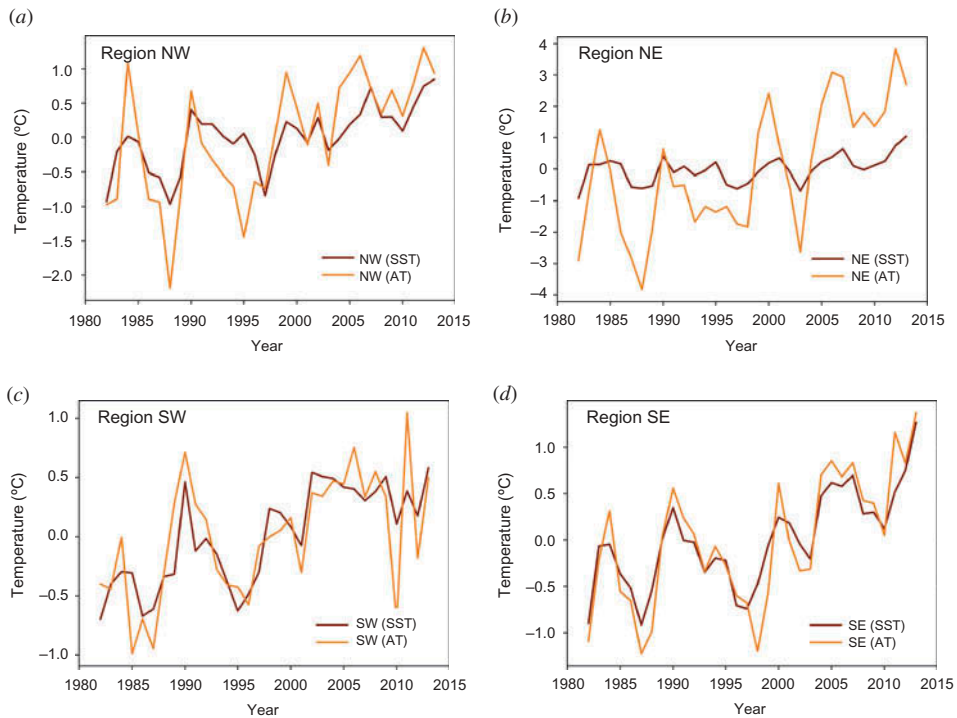


Figure 13. Comparison of the annual SST and AT anomalies: (a) region NW, (b) region NE, (c) region SW, and (d) region SE.

correlation between SW and NE regions is the lowest ( $r = 0.42$ ). Similar results have been obtained for the AT anomalies (Figures 14(d)–(f)). The highest correlation is between the ATs in the SW and SE regions ( $r = 0.69$ ), and the lowest for the ATs in the SW and NE regions ( $r = 0.48$ ). The correlations between the SST and AT anomalies in the same regions (Figures 15(a)–(d)) are even higher (ranging between  $r = 0.94$  in the SE region

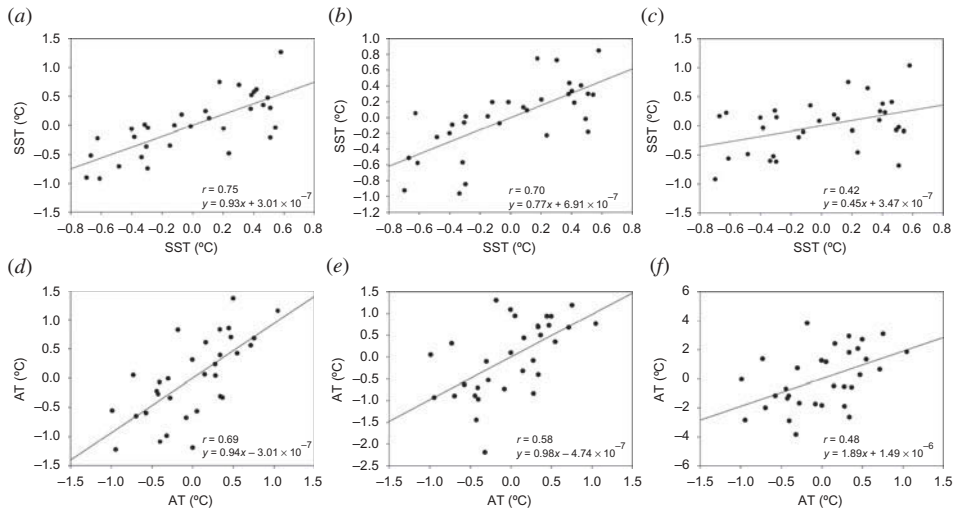


Figure 14. Temperatures in different regions plotted as a function of temperatures in the SW region: (a) and (d) SE region versus SW region, (b) and (e) NW region versus SW region, (c) and (f) NE region versus SW region. Top panels (a)–(c) are for the annual SST anomalies, and bottom panels (d)–(f) are for the annual AT anomalies.

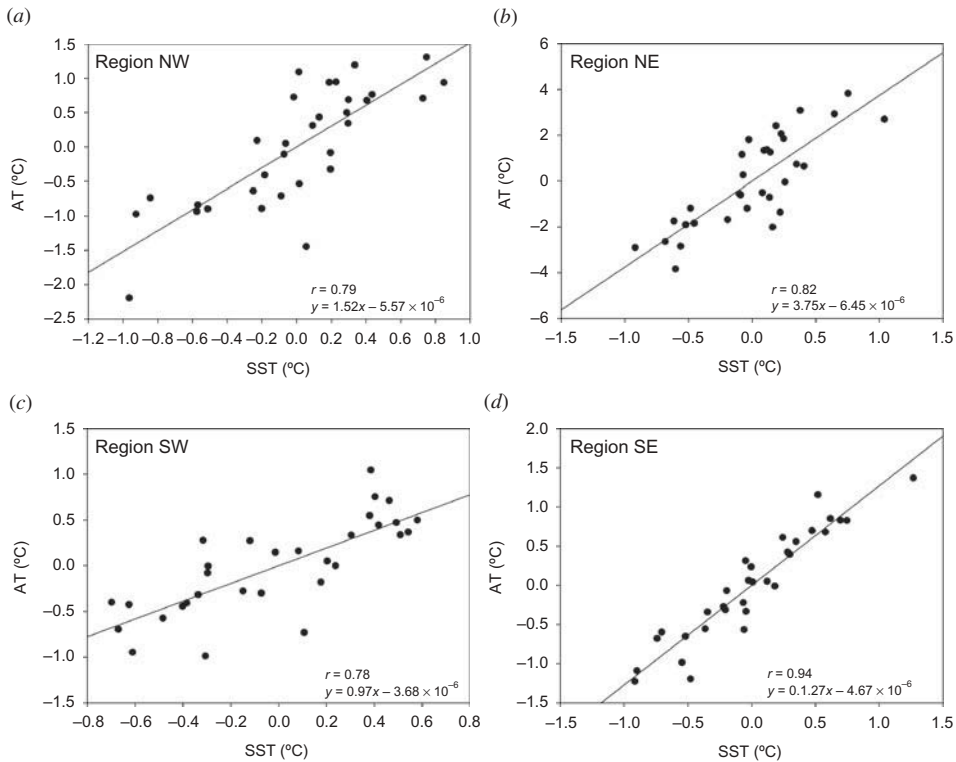


Figure 15. Correlations between the annual regionally averaged SST and AT anomalies in (a) NW region, (b) NE region, (c) SW region, and (d) SE region.

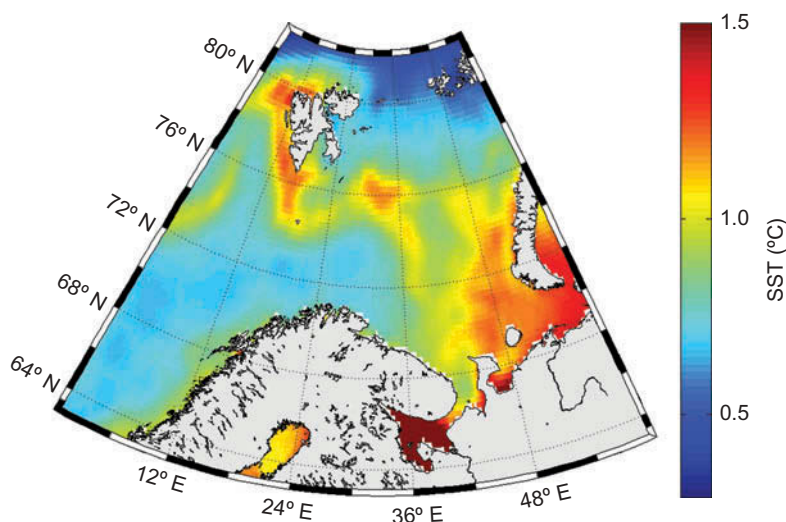


Figure 16. Map of the SDs calculated from the daily SST data, after subtracting the multi-year trend and the average annual cycle.

and  $r = 0.78$  in the SW region). All the correlations shown in Figures 14 and 15 are statistically significant ( $p < 0.05$  at 95% confidence level).

In Figure 16, we have plotted spatial patterns in the SDs of the daily SST anomalies. The SDs were calculated after subtracting the seasonal cycle and the multi-year trends from the daily SST data. These SD estimates allow us to assess the overall SST variability not explained by the seasonal cycle and multi-year trends. The highest values of the SDs are detected near the Svalbard Archipelago and Novaya Zemlya, as well as in the coastal regions near the Eurasian coast, where SD values are about  $1.35^{\circ}\text{C}$ . The lowest SDs are noted in the region of the AW inflow (about  $0.75^{\circ}\text{C}$ ).

#### 4. Summary and conclusions

In this study, we have used the 32 year long satellite-derived SST data to investigate the warming trends in the BS. Our results support the notion that regionally averaged SST trend in the BS is greater than the global trend. Averaged trend for the entire BS ( $0^{\circ}\text{E}$   $62.875^{\circ}\text{N}$  and  $59.875^{\circ}\text{E}$   $82.375^{\circ}\text{N}$ ) based on the data from 1982 to 2013 has been estimated as about  $0.03^{\circ}\text{C year}^{-1}$ . The fact that the SST trend in the BS is greater than the globally averaged trend is consistent with the Arctic amplification of the global warming debated broadly in the literature (e.g. Comiso and Hall 2014). The trend for the annually averaged SST in the BS varies spatially, with the lowest values in the area located north from  $76^{\circ}\text{N}$  and the highest values exceeding  $0.06^{\circ}\text{C year}^{-1}$  in the region located near the Svalbard Archipelago and in the coastal regions near the White Sea. Large SST trends observed in the coastal regions can be associated with increasing freshwater run-off from the land. This run-off increases the water column stratification in the ocean and supplies more terrigenous material, increasing the absorption of light and heating the surface waters.

The estimated SST trend is particularly high in the winter months in the open BS region located west from Novaya Zemlya. The same region is characterized by stronger than BS averaged trend of the AT. This is associated with the fact that in this region a

significant retreat of the sea ice has been observed in recent years, which must have been accompanied by a significant decrease in the sea-surface albedo and more efficient warming of surface waters. At the present time, we do not have appropriate data to investigate the forcing mechanisms responsible for the observed SST trends. In general, the trends could be attributed to changes in the ocean circulation and/or changes in the air–sea heat fluxes. There is an ongoing discussion about the trends in the volume transport and temperature of the AW transported with the North Atlantic Current (e.g. Beszczynska-Moller et al. 2012). A link between the AW temperature anomalies in the transition zone between the NAC and the West Spitsbergen current and the surface heat flux anomalies over the BS open waters has been suggested by Schlichtholz and Houssais (2011). Another possible mechanism behind the observed increase in SST is related to changes in the optical properties of surface waters, for example due to increased concentrations of coloured organic dissolved matter or suspended particles. This is because the local heating rate depends not only on the amount of solar radiation incident on the sea surface but also on the vertical distribution of irradiance in the water column (e.g. Stramska and Zuzewicz 2013). More research is needed to fully investigate the relative importance of these processes in the BS.

Variability of the SST in the BS is characterized by considerable amplitude of the seasonal cycle, which exceeds 8°C in the coastal regions (near Norway, Kola peninsula, northern parts of Russia) and is about 6–7°C in the shallow section of the BS where the water depth is below 200 m. The smallest amplitude of the 32 year averaged annual SST cycle is observed in the West Spitsbergen Current (about 3°C) and in the northern regions. The annual cycle is asymmetric, with the time period when the SSTs are lower than the annual average longer than the time period when the SSTs are higher than the annual average. Annually averaged SSTs are undergoing a considerable interannual variability, which has similar temporal patterns in different parts of the BS. The interannual patterns of SST variability in the three study regions (NW, SE, NE) were significantly correlated with the interannual patterns of SST observed in the SW region influenced by the NAC; however, in the NE region characterized by significant sea-ice fraction, the correlation coefficient is significantly smaller than in other regions. The interannual patterns in the AT are well correlated with the interannual patterns in the SST in all four regions. The 32 year averaged daily AT time series assumed most of the time lower values than the 32 year averaged daily SST time series in all study regions, emphasizing the notion that this region transfers significant amount of heat from the sea surface to the atmosphere.

The degree of change of climate is currently the subject of much debate. One of the important environmental parameters that can be used to track climate change is the SST (e.g. Deser et al. 2010). It is important to estimate trends in SST on global and regional scales accurately in order to document and improve the understanding of the climate change. Although in comparison to *in situ* measurements the satellite observations span relatively short time periods, these data sets have the advantage that they provide good spatial ocean coverage, allowing spatial patterns in SST trends to be determined. Improved understanding of the SST trends and their relationships with AT and sea-ice coverage can provide critical information about the impacts of the Earth's climate on the status of the BS.

### Acknowledgements

We are grateful to the NOAA/OAR/ESRL PSD, Boulder, Colorado, and the NOAA-CIRES Climate Diagnostic Center NCEP/NCAR for making available the data sets used in this study.

## Funding

This work was funded by the Norway Grants through the Polish-Norwegian Research Programme operated by the National Centre for Research and Development (NCBR contract No. 201985 entitled ‘Application of in situ observations, high frequency radars, and ocean color, to study suspended matter, particulate carbon, and dissolved organic carbon fluxes in coastal waters of the Barents Sea’).

## References

- Ådlandsvik, B., and H. Loeng. 1991. “A Study of the Climatic System in the Barents Sea.” *Polar Research* 10: 45–50. doi:10.1111/j.1751-8369.1991.tb00633.x.
- Bengtsson, L., V. A. Semenov, and O. M. Johannessen. 2004. “The Early Twentieth-Century Warming in the Arctic—A Possible Mechanism.” *Journal of Climate* 17: 4045–4057. doi:10.1175/1520-0442(2004)017<4045:TETWIT>2.0.CO;2.
- Beszczynska-Moller, A., E. Fahrbach, U. Schauer, and E. Hansen. 2012. “Variability in Atlantic Water Temperature and Transport at the Entrance to the Arctic Ocean 1997-2010.” *ICES Journal of Marine Science* 69: 2281–2298. doi:10.1093/icesjms/fss056.
- Comiso, J. C., and D. K. Hall. 2014. “Climate Trends in the Arctic as Observed from Space.” *Wiley Interdisciplinary Reviews: Climate Change* 5: 389–409. doi:10.1002/wcc.277.
- Deser, C., M. A. Alexander, S.-P. Xie, and A. S. Phillips. 2010. “Sea Surface Temperature Variability: Patterns and Mechanisms.” *Annual Review of Marine Science* 2: 115–143. doi:10.1146/annurev-marine-120408-151453.
- Fichot, C. G., K. Kaiser, S. B. Hooker, R. M. W. Amon, M. Babin, S. Bélanger, S. A. Walker, and R. Benner. 2013. “Pan-Arctic Distributions of Continental Runoff in the Arctic Ocean.” *Scientific Reports* 3: 1053. doi:10.1038/srep01053.
- Good, S. A., G. K. Corlett, J. J. Remedios, E. J. Noyes, and D. T. Llewellyn-Jones. 2007. “The Global Trend in Sea Surface Temperature from 20 Years of Advanced Very High Resolution Radiometer Data.” *Journal of Climate* 20: 1255–1264. doi:10.1175/JCLI4049.1.
- Ikeda, M. 1990. “Decadal Oscillations of the Air-Ice-Ocean System in the Northern Hemisphere.” *Journal of Atmospheric and Oceanic Technology* 28: 106–139. doi:10.1080/07055900.1990.9649369.
- Ikeda, M., J. Wang, and J.-P. Zhao. 2001. “Hypersensitive Decadal Oscillations in the Arctic/Subarctic Climate.” *Geophysical Research Letters* 28: 1275–1278. doi:10.1029/2000GL011773.
- Lesack, L., P. Marsh, F. Hicks, and D. Forbes. 2014. “Local Spring Warming Drives Earlier River-Ice Breakup in a Large Arctic Delta.” *Geophysical Research Letters* 41: 1560–1567. doi:10.1002/2013GL058761.
- Liang, X., and A. Ignatov. 2011. “Monitoring of IR Clear-Sky Radiances over Oceans for SST (MICROS).” *Journal of Atmospheric and Oceanic Technology* 28: 1228–1242. doi:10.1175/JTECH-D-10-05023.1.
- Loeng, H. 1991. “Features of the Physical Oceanographic Conditions of the Barents Sea.” *Polar Research* 10: 5–18. doi:10.1111/j.1751-8369.1991.tb00630.x.
- Maslowski, W., D. Marble, W. Walczowski, U. Schauer, J. L. Clement, and A. J. Semtner. 2004. “On Climatological Mass, Heat, and Salt Transports through the Barents Sea and Fram Strait from a Pan-Arctic Coupled Ice Ocean Model Simulation.” *Journal of Geophysical Research* 109: C03032. doi:10.1029/2001JC001039.
- Midttun, L. 1985. “Formation of Dense Bottom Water in the Barents Sea.” *Deep Sea Research Part A. Oceanographic Research Papers* 32: 1233–1241. doi:10.1016/0198-0149(85)90006-8.
- Morison, J., R. Kwok, C. Peralta-Ferriz, M. Alkire, I. Rigor, R. Andersen, and M. Steele. 2012. “Changing Arctic Ocean Freshwater Pathways.” *Nature* 481: 66–70. doi:10.1038/nature10705.
- Nghiem, S. V., D. K. Hall, I. G. Rigor, P. Li, and G. Neumann. 2014. “Effects of Mackenzie River Discharge and Bathymetry on Sea Ice in the Beaufort Sea.” *Geophysical Research Letters* 41: 873–879. doi:10.1002/2013GL058956.
- Ostasiewicz, S., Z. Rusnak, and U. Siedlecka. 2006. *Statystyka: Elementy Teorii i Zadania*. [in Polish.] Wrocław: Wrocław University of Economics Publishing House.
- Peterson, B. J., R. M. Holmes, J. W. McClelland, C. J. Vörösmarty, R. B. Lammers, A. I. Shiklomanov, I. A. Shiklomanov, and S. Rahmstorf. 2002. “Increasing River Discharge to the Arctic Ocean.” *Science* 298 (5601): 2171–2173. doi:10.1126/science.1077445.

- Reynolds, R. W., T. M. Smith, C. Liu, D. B. Chelton, K. S. Casey, and M. G. Schlax. 2007. "Daily High-Resolution-Blended Analyses for Sea Surface Temperature." *Journal of Climate* 20: 5473–5496. doi:10.1175/2007JCLI1824.1.
- Rudels, B., E. P. Jones, U. Schauer, and P. Eriksson. 2004. "Atlantic Sources of the Arctic Ocean Surface and Halocline Waters." *Polar Research* 23 (2): 181–208. doi:10.1111/j.1751-8369.2004.tb00007.x.
- Sandø, A. B., J. E. Ø. Nilsen, Y. Gao, and K. Lohmann. 2010. "Importance of Heat Transport and Local Air Sea Heat Fluxes for Barents Sea Climate Variability." *Journal of Geophysical Research* 115: C07013. doi:10.1029/2009JC005884.
- Schauer, U., A. Beszczynska-Möller, W. Walczowski, E. Fahrbach, J. Piechura, and E. Hansen. 2008. "Variation of Measured Heat Flow through the Fram Strait between 1997 and 2006." In *Arctic Subarctic Ocean Fluxes: Defining the Role of the Northern Seas in Climate*, edited by R. R. Dickson, J. Meincke, and P. Rhines, 65–85. New York: Springer.
- Schauer, U., H. Loeng, B. Rudels, V. K. Ozhigin, and W. Dieck. 2002. "Atlantic Water Flow through the Barents and Kara Seas." *Deep Sea Research Part I: Oceanographic Research Papers* 49: 2281–2298. doi:10.1016/S0967-0637(02)00125-5.
- Schlichtholz, P. 2011. "Influence of Oceanic Heat Variability on Sea Ice Anomalies in the Nordic Seas." *Geophysical Research Letters* 38: L05705. doi:10.1029/2010GL045894.
- Schlichtholz, P., and M.-N. Houssais. 2011. "Forcing of Oceanic Heat Anomalies by Air-Sea Interactions in the Nordic Seas Area." *Journal of Geophysical Research* 116: C01006. doi:10.1029/2009JC005944.
- Serreze, M., A. Barrett, A. Slater, M. Steele, J. Zhang, and K. Trenberth. 2007. "The Large-Scale Energy Budget of the Arctic." *Journal of Geophysical Research* 112: 1438–1445. doi:10.1029/2006JD008230.
- Stramska, M., and A. Zuzewicz. 2013. "Influence of the Parametrization of Water Optical Properties on the Modelled Sea Surface Temperature in the Baltic Sea." *Oceanologia* 55 (1): 53–76. doi:10.5697/oc.55-1.053.